Ultrashort Echo Time Imaging of the Lungs Under High-Frequency Noninvasive Ventilation: A New Approach to Lung Imaging

Jean Delacoste, PhD,[1] Gael Dournes, MD, PhD,[2,3,4] Vincent Dunet, MD,[1*]

Adam Ogna, MD,[5,6] Leslie Noirez, MD,[5] Julien Simons, BS,[7] Olivier Long, BS,[7]

Grégoire Berchier, BS,[1] Matthias Stuber, PhD,[1,8] Alban Lovis, MD,[5] and

Catherine Beigelman-Aubry, MD[1]

Background: Although ultrashort echo time (UTE) sequences allow excellent assessment of lung parenchyma, image quality remains lower than that of computed tomography (CT).
Purpose: To investigate a high-frequency noninvasive ventilation (HF-NIV) technique allowing a stabilized inspiration and to compare image quality with current dedicated MR sequences.
Study Type: Prospective.
Population: Ten healthy volunteers.
Field Strength/Sequence: 3D radial UTE sequence at 1.5T.
Assessment: UTE-HF-NIV sequence was compared with UTE-free-breathing (UTE-FB), reconstructed at end expiration (UTE-Exp) and average (UTE-Avg), and breath-hold VIBE sequences. The distance from lung apex to the dome of the right hemidiaphragm was measured. Visual assessment of the visibility and sharpness of normal anatomical structures was carried out. Dedicated software also quantitatively evaluated vessel–lung and right lung–liver interface sharpness. Apparent signal ratio (Sr) and contrast ratios (Cr) were quantitatively evaluated.
Statistical Tests: Wilcoxon signed rank test for visual scores, paired t-test for continuous variables, significance at $P < 0.05$.
Results: The distance between apex and the right hemidiaphragmatic dome was significantly larger ($P < 0.001$) with UTE-HF-NIV compared with UTE-FB and VIBE acquisitions. Vessel and airway visibility had identical median visual scores with all UTE methods. Median visual scores for sharpness of vessels and airways were significantly higher ($P < 0.001$) with HF-NIV (vessels = 3; airways = 2) than in UTE-FB (vessels = 2; airways = 1) and VIBE (vessels = 1; airways = 1). Software-based vessel sharpness evaluation resulted in larger values in 8/10 volunteers with UTE-HF-NIV (67.3 ± 9.8) compared with UTE-Avg (62.3 ± 12.6) but the average difference was not significant ($P = 0.28$). The sharpness of the lung–liver interface was significantly higher ($P < 0.001$) with HF-NIV (17.3 ± 5.3) compared with UTE-Avg (14.1 ± 3.9). Significantly higher values ($P < 0.01$) of Sr and Cr were observed with UTE-HF-NIV compared with UTE-FB and VIBE.
Data Conclusion: HF-NIV allowing acquisition at full inspiration significantly improves image quality for lung imaging. This could offer the option to alternate some follow-up CT studies by using this technique.
Level of Evidence: 2
Technical Efficacy: Stage 1

*Address reprint requests to: V.D., Department of Diagnostic and Interventional Radiology, Centre Hospitalier Universitaire Vaudois (CHUV), Rue du Bugnon 46, 1011 Lausanne, Switzerland. E-mail: vincent.dunet@chuv.ch
The last two authors contributed equally to this work.

From the [1]Department of Diagnostic and Interventional Radiology, University Hospital (CHUV) and University of Lausanne (UNIL), Lausanne, Switzerland; [2]Centre de Recherche Cardio-Thoracique de Bordeaux, University of Bordeaux, Bordeaux, France; [3]Centre de Recherche Cardio-Thoracique de Bordeaux, Inserm, Bordeaux, France; [4]CHU de Bordeaux, Service d'Imagerie Thoracique et Cardiovasculaire, Service des Maladies Respiratoires, Service d'Exploration Fonctionnelle Respiratoire, Pessac, France; [5]Department of Pneumology, University Hospital (CHUV) and University of Lausanne (UNIL), Lausanne, Switzerland; [6]Departement of Respiratory Medicine, Ospedale La Carità, Locarno, Switzerland; [7]Department of Physiotherapy, CHUV and University of Lausanne, Lausanne, Switzerland; and [8]Center for Biomedical Imaging (CIBM), Lausanne, Switzerland

THE RAPID DECAY of signal in the lung parenchyma makes magnetic resonance imaging (MRI) of the lung challenging. The development of ultrashort echo time (UTE) acquisition has enabled obtaining sufficient signal in the parenchyma despite the short T_2*,[1] while recent technical developments have allowed 3D acquisitions with high spatial resolution.[2] Multiple studies have demonstrated nowadays an interest in noncontrast-enhanced UTE for the evaluation of various pulmonary and airway disorders, including nodules or masses, ground glass opacity, micronodules, nodules, patchy shadow or consolidation, emphysema or bullae, bronchiectasis, reticular opacity, honeycomb, and traction bronchiectasis.[3–6] Besides pulmonary disease, UTE imaging has also been evaluated in other regions of the body, with a potential in qualitative and quantitative assessment in the musculoskeletal system,[7] but without current use in routine practice.

Although UTE sequences[1] allow an excellent assessment of lung parenchyma,[8,9] image quality remains lower than that obtained by computed tomography (CT). CT remains the first modality for lung imaging, but the use of MRI as a radiation-free alternative remains attractive and needs to be further explored in the light of recent developments in hardware and software. Although 3D radial UTE sequences allow full chest coverage with isotropic spatial resolution, acquisition in a single breath-hold is challenging.[2] For this reason, such sequences are typically acquired during free-breathing using respiratory gating or triggering.[2] While free-breathing acquisitions allow insight into lung function,[10] the chest structures remain at tidal volume rather than at the an end-inspiratory volume required for CT imaging. Indeed, nodules may be missed especially at the base of the lungs if this condition is not fulfilled.[11] In addition, even though some MRI sequences dedicated to lung imaging allow segmentation of the acquisition in multiple breath-holds,[12] this increases operator involvement and patient fatigue. Moreover, the lung volume at breath-hold is commonly imperfectly reproduced, leading to misregistration artifacts.[13,14] A technique allowing high-resolution MRI of the lung at an end-inspiratory volume could approach the appearance of CT, facilitating intermodality comparison, and thus make it a viable alternative in clinical practice. High-frequency noninvasive ventilation (HF-NIV) has been recently applied to achieve respiratory stabilization at inspiratory volume during multiple minutes for radiotherapy[15] and an initial pilot study subsequently demonstrated the feasibility of this technique for MRI.[16] However, a systematic evaluation of the image quality obtained with this new technique remains to be carried out. One goal of the present study was to confirm the difference in organ positions when HF-NIV was used compared with current dedicated MR sequences for lung imaging, especially at the diaphragmatic level. Further, we also quantified the image quality achieved with this new method.

Materials and Methods

Data Acquisition and Reconstruction

Data were acquired in 10 healthy volunteers (seven male, three female subjects [age 21–43], mean 32 years old) using a prototype double echo UTE sequence[17,18] with spiral phyllotaxis trajectory.[19] All volunteers provided written informed consent before examination in this Ethics Committee-approved study. Acquisition was carried out on a 1.5T clinical scanner (Magnetom Aera, Siemens Healthcare, Erlangen, Germany) equipped with an 18-element body coil and 24-element spine coil. Acquisition parameters were TE_1 = 0.05 msec, TE_2 = 2.86 msec, pulse repetition time (TR) = 5.9 msec, readout $bandwidth_1$ = 303 Hz/pixel, readout $bandwidth_2$ = 606 Hz/pixel, RF excitation angle = 5°, field of view = 500 mm^3, matrix size = 384^3, voxel size = 1.3 mm^3, and 602 segments consisting of 100 readouts each. No triggering or gating was used during data acquisition.

For each volunteer, the UTE acquisition was carried out during a 6-minute long respiratory stabilization period. Stabilization was achieved with HF-NIV using a Monsoon III ventilator (Acutronic Medical Systems, Hirzel, Switzerland) and a noninvasive patient interface (Phasitron; Percussionaire, Sandpoint, ID)[16] at a respiratory rate of 250 per minute as previously published.[20] In summary, subjects were ventilated delivering small tidal volumes, around 50 ml, at high frequency, which allows supporting gas exchange, in particular CO_2 clearing, and thus limits the need to breathe. Compared with the previously described technique, the length of the ventilator circuit had to be extended up to 6 m to install the Monsoon ventilator in the MRI control room. This adaptation reduces the efficacy of ventilation limiting the duration of apnea, from more than 20 minutes for the original 2-m circuit down to ~6 minutes for a 6-m circuit.[21] A training ventilation session was performed with each subject before the MRI session.

In addition to the UTE-HF-NIV acquisition, a free-breathing UTE acquisition (UTE-FB) was performed to obtain motion-averaged datasets and retrospectively gated end-expiration datasets.

This sequence was chosen for comparison as it could be acquired with identical imaging parameters as during HF-NIV.

UTE images were first reconstructed for both acquisitions (UTE-FB and UTE-HF-NIV) using nonuniform fast Fourier transform and all the acquired data. For UTE-FB acquisitions, this yielded motion-averaged datasets (UTE-Avg). Additionally, UTE-FB data were also reconstructed using a compressed sensing algorithm exploiting sparsity over the respiratory dimension in order to obtain respiratory-motion-resolved image volumes.[22] Four image volumes, spanning from end-expiration to end-inspiration of tidal breathing, were reconstructed for each free-breathing acquisition. The end-expiratory images were used for analysis (UTE-Exp).

In addition, standard 3D gradient echo acquisition was carried out during an unassisted breath-hold using the VIBE (volumetric interpolated breath-hold examination) acquisition with asymmetric sampling in the readout dimension. Acquisition parameters were as follows: TE = 0.81 msec, TR = 3.07 msec, field of view = 400 × 300 mm, pixel resolution = (1.04 mm)^2, 72 slices, slice thickness = 4 mm.

The ordering of the acquisitions was randomly defined and 6/10 MR protocols were performed using HF-NIV after free-breathing acquisition, while 4/10 were performed using HF-NIV before free-breathing acquisition. All free-breathing and breath-hold acquisitions were performed after resumed normal breathing.

Image Analysis

The distance from the lung apex to the dome of the right hemidiaphragm was measured in the free-breathing images and those acquired with HF-NIV for each subject.

Image quality was scored visually, integrating the visibility of normal anatomical structures in, respectively, the vessels, bronchi, and fissures. Images were reviewed in consensus in the axial orientation for vessels and airways and in coronal orientation for assessment of fissures by two experts in chest imaging with 25 (C.B.A.) and 8 (G.D.) years of experience in thoracic imaging. The experts were blinded to the method used for image acquisition. Recall bias was minimized by separating readings of HF-NIV and free-breathing data by 3 weeks. A third reader (V.D.), blinded from consensus results, independently evaluated the five first participants' images 6 months later. The five first participants' images were therefore independently evaluated twice (two readers in consensus vs. a third reader 6 months later).

Pulmonary vasculature visibility was scored separately for the central part of the lung in each segment, using a modification of the score by Ohno et al[23] for both vessels and airways: 1 = no depiction; 2 = depicted at segmental level; 3 = depicted at subsegmental level; 4 = depicted at sub-subsegmental level; 5 = depicted beyond sub-subsegmental level. Fissure visibility was scored as follows: 1 = not visible; 2 = visible. Peripheral vessels, defined as the external third of the chest, were scored as 1 = not visible; 2 = visible. There was no attempt to score the visibility of bronchi in the peripheral part of the lung.

Subsequently, sharpness of interfaces of visible bronchi, vessels, and fissures was scored using the following discrete scale: 1 = blurred; 2 = intermediate; 3 = sharp. Artifacts were given a score between 1 and 4 as follows: 1 = severe artifact with no normal structure recognizable; 2 = moderate artifact with blurring of anatomical structures; 3 = slight artifact without blurring of anatomical structures; 4 = no artifact.

The sharpness of vessels was also quantified on UTE-HF-NIV and UTE-Avg images using Soapbubble, a dedicated software algorithm that measures first-order derivatives at tissue interfaces.[24] This algorithm, widely used in cardiovascular imaging studies, has been recently used in lung imaging studies. As in previous studies,[17] the analysis was performed at the level of a segmental artery, in our case the right postero-basal segmental artery and percent vessel sharpness is reported. Similarly, the sharpness of the right lung–liver interface was also quantified on UTE-HF-NIV and UTE-Avg images with a method adapted from the one originally introduced by Tibiletti et al[25] and that has since been used in multiple lung imaging studies.[17,26] First, 21 vertical profiles going through the lung–liver interface were defined on coronal slices. These profiles were then filtered with a median filter (filter width = 10) and the derivative was computed along each profile. The maximum value of the derivative was then divided by the signal intensity range to obtain a sharpness ratio, expressed as a percentage.

Lung signal intensity was also assessed quantitatively.[27] Briefly, circular regions of interest (ROIs) of the same size were manually placed by two independent observers in the axial plane. ROIs corresponding to signal intensity (SI) within air were placed in the trachea and in the right and left main bronchus, and data in these ROIs were averaged to calculate SI_{airway}. ROIs corresponding to SI within vessels were traced in the pulmonary trunk and in the right and left main pulmonary arteries, and data in these ROIs were averaged to

calculate SI_{vessel}. Regarding the assessment of SI in the lung parenchyma, three axial sections were selected: one at the level of the aortic arch, one at the level of the carina, and one at the level of the lower pulmonary veins. ROIs were placed at each location in the anterior part and posterior part of the right and left lungs, respectively, at least 2 cm from the lung periphery. Vessels were carefully avoided when ROIs were traced. Data in the 12 resulting ROIs were averaged to calculate SI_{lung}. The mean value between readers was used for analysis. The apparent contrast ratio (Cr) and signal ratio (Sr) were calculated, as follows[27]: $Cr = (SI_{lung} - SI_{airway})/SI_{vessel} \cdot 100\%$ and $Sr = (SI_{lung}/SI_{airway}) \cdot 100\%$.

Clinical Tolerance

At the end of the imaging sessions, participants were asked to rate subjectively the level of discomfort felt during HF-NIV acquisition by reporting an integer value ranging between 0 (no discomfort) and 5 (extreme discomfort).

Statistical Assessment

Statistical analysis was carried out using R v. 3.4.0 with the ggpubr package v. 0.1.6 (https://cran.r-project.org/package = ggpubr). A Kruskal–Wallis test by ranks was used to evaluate the visual scores. To complement the global information obtained with the Kruskal–Wallis test, when this test indicated the existence of a significant difference, pairwise comparison was additionally carried out using a Wilcoxon signed rank test with Holm's correction for multiple comparisons.[28] For continuous variables, an analysis of variance (ANOVA) test was used to evaluate differences in the data, and was followed by pairwise Student's paired t-test with Holm's correction for multiple comparisons. In all cases, $P < 0.05$ was considered statistically significant.

To assess interobserver reliability of the subjective scoring, we used the Gwet AC1, which is less dependent on marginal distribution than Cohen's kappa, marginal distribution affecting the calculation of chance-corrected agreement coefficient.[29,30] Interobserver reliability was assessed for each item combining right and left lungs ($n = 10$) for fissures' items and artifacts, and right and left segments ($n = 90$) for vessels and airways' items, on breath-hold VIBE, UTE-Exp, and UTE-HF-NIV sequences. The Landis and Koch scale was used to characterize the value of the Gwet's AC1 coefficient, as follows: poor when Gwet's AC1 was <0.00, slight between 0.00 and 0.20, fair between 0.21 and 0.40, moderate between 0.41 and 0.60, good between 0.61 and 0.80 and excellent above 0.81.

Results

The procedure was well tolerated by all subjects. The subjective tolerance score was evaluated in eight of the ten subjects: Three subjects reported subjective discomfort scores of 1, three subjects reported a score of 2, and two subjects reported a score of 3 (median = 2).

A significantly larger distance between apex and right hemidiaphragmatic dome (Fig. 1a) was observed when using UTE-HF-NIV (22.3 ± 3.1 cm) compared with both UTE free-breathing methods, UTE-Avg and UTE-Exp (16.2 ± 2.5 cm and 15.5 ± 2.2 cm, respectively, $P < 0.001$) and compared with the VIBE method (20.0 ± 2.3 cm, $P < 0.005$).
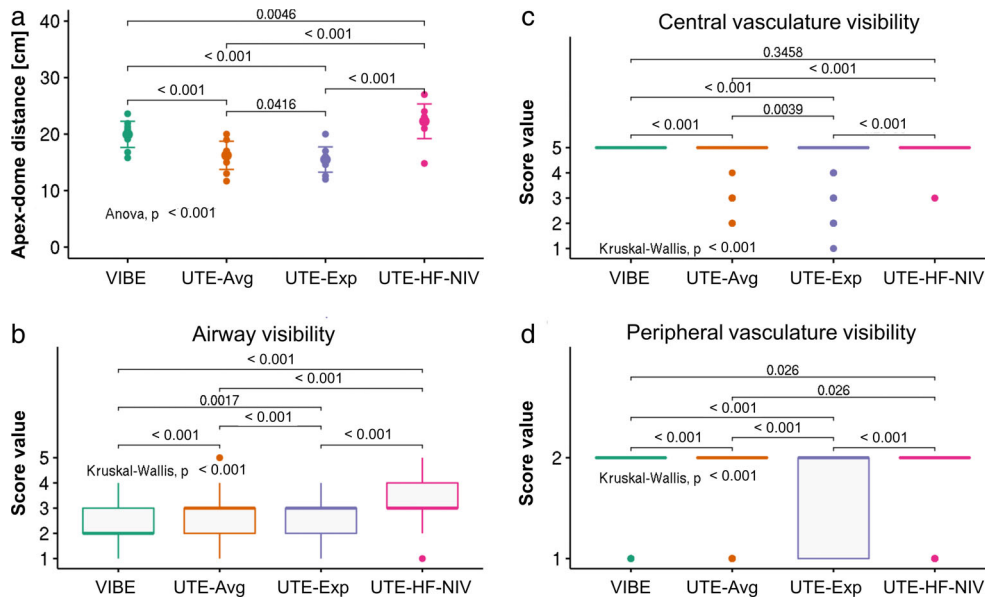
FIGURE 1: (a) The average distance from lung apex to dome of right hemidiaphragm was significantly increased with the use of HF-NIV (error bars indicate standard deviation). (b) The median value (thick line) of the visibility score was identical between all UTE acquisition and reconstruction methods for airways (b), and between all methods for central vasculature (c) and peripheral vasculature (d). Upper and lower boundaries of boxes indicate the 25% and 75% quantiles, respectively. In particular, the interquartile range of airway visibility scores included higher values when HF-NIV was used.

Interobserver reliability was excellent for all items on VIBE and UTE-HF-NIV sequences (all Gwet AC1 ≥ 0.91, $P < 0.001$). For UTE-Exp the interobserver reliability was excellent (Gwet AC1 ≥ 0.97, $P < 0.001$) for all items except for artifacts (Gwet AC1 = 0.80[0.36–1.0], $P = 0.003$) and peripheral vessel visibility (Gwet AC1 = 0.76[0.62–0.90], $P < 0.001$), for which interobserver reliability was good.

Airway visibility had identical median visual scores when acquisition was performed with UTE-HF-NIV compared with UTE FB methods even though the interquartile range (IQR) included higher scores with HF-NIV (IQR = [3 4]) compared with FB (IQR = [2 3], Fig. 1b). Conversely, the VIBE presented a significantly lower median score value in comparison with UTE-HF-NIV (median score = 2, IQR = [2 3]). Both central and peripheral vasculature visibility resulted in identical median visual scores for all methods (Fig. 1c,d). Fissure visibility had a median score of 1 with all methods (UTE-HF-NIV IQR = [1 2]; UTE-Avg IQR = [1 1.25]; UTE-Exp IQR = [1 1]; VIBE IQR = [1 1]).

Visual scores for sharpness of vessels (Fig. 2a,b) and airways (Fig. 2c) were significantly higher ($P < 0.001$) in images acquired with UTE-HF-NIV respiratory stabilization than in those acquired during UTE-FB and VIBE. Fissure sharpness could not be statistically assessed in our paired design, as sharpness assessment was always absent for at least one modality, due to fissures not being visible.

Software-based vessel sharpness evaluation resulted in larger values in 8/10 volunteers when UTE-HF-NIV was used compared with UTE-Avg, but the average difference was not significant (Fig. 2d). The sharpness of the lung–liver interface (Fig. 2e) was higher in 8/10 volunteers (same individuals as for

the vessel sharpness measurement) when UTE-HF-NIV was used (17.3 ± 5.3) compared with UTE-Avg (14.1 ± 3.9) and the overall average difference was significant ($P < 0.001$).

The visual score for artifacts was higher but not significantly ($P = 0.15$) when UTE-HF-NIV was used (median score = 2.5; IQR = [2 3]) compared with UTE-Avg (median score = 2; IQR = [1 3]), while it was identical to the visual score for artifacts obtained with the VIBE ($P > 0.05$) and slightly lower than that obtained with the UTE-Exp but not significantly (median score = 3; IQR = [2 3]; $P > 0.05$).

A significantly higher average signal was measured in the parenchyma (SI_{lung}) in the UTE-HF-NIV images compared with UTE-Exp and UTE-Avg images ($P = 0.005$ and $P = 0.04$, respectively, Fig. 3a). The SI_{lung} in the UTE-HF-NIV images was as well higher than that in the VIBE images, yet not significantly ($P > 0.1$). The average SI_{vessel} value in UTE-HF-NIV images was significantly higher than the SI_{vessel} value in UTE-Exp images and significantly lower than SI_{vessel} value in VIBE images ($P = 0.045$ and $P = 0.001$, respectively, Fig. 3b) while no significant differences were observed in average SI_{airway} among all methods (Fig. 3c). These quantitative evaluations resulted in significantly higher ($P < 0.01$) values for the apparent signal ratio (Fig. 3d) and contrast ratio (Fig. 3e) when UTE-HF-NIV was used for image acquisition compared with the UTE-Avg, UTE-Exp, and VIBE methods.

These results were appreciated visually. For all volunteers, the difference in lung inflation was clearly apparent (Fig. 4). The sharpness increase when using UTE-HF-NIV could also be seen over the entire field of view in most volunteers (eg, Figs. 4–5). In the 2/10 cases, where the software-based sharpness evaluation did not point to a sharpness
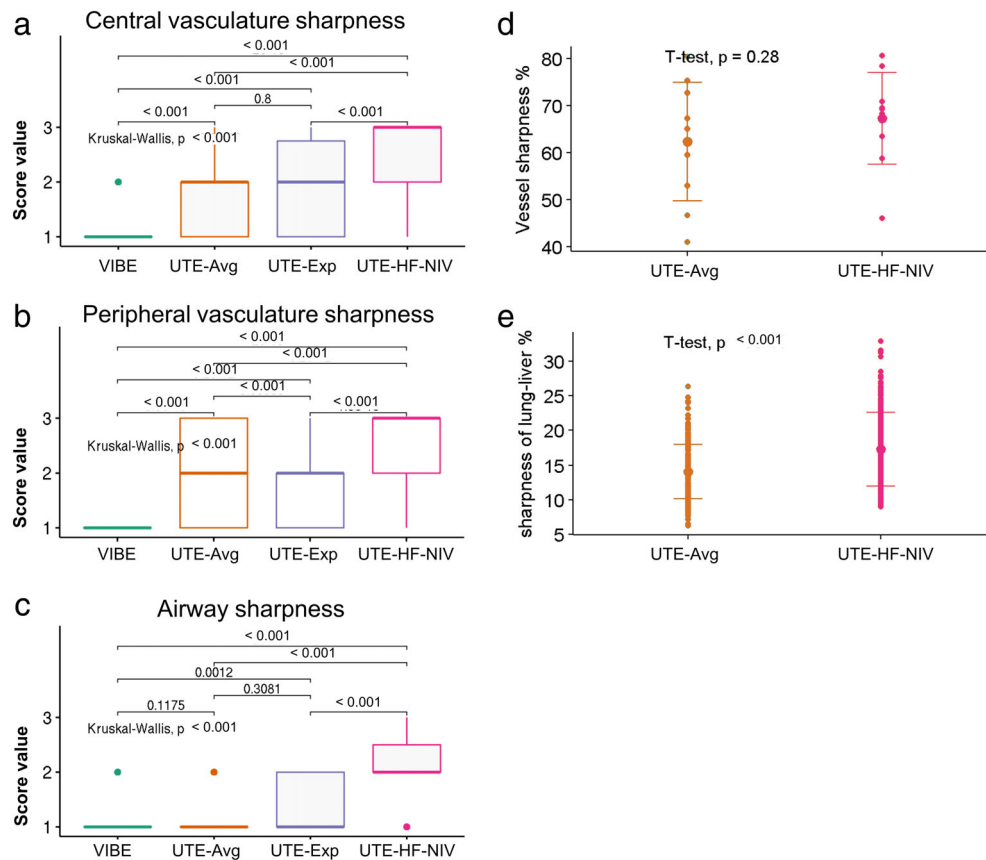
FIGURE 2: Visual evaluation of sharpness indicated significant increases for central vasculature (a), peripheral vasculature (b), and airways (c). Thick line indicates median, while upper and lower boundaries of boxes indicate the 25% and 75% quantiles, respectively. Software-based quantification of vessel sharpness indicated a trend to an increase but was not significant (d). However, the average lung–liver interface sharpness was significantly increased with the use of HF-NIV (e). Error bars indicate standard deviation.

increase, blurring was more apparent in the UTE-HF-NIV images, as seen, for example, in Fig. 4.

Discussion

Although numerous efforts have been made for the development of lung MRI, to this date CT remains predominantly the reference modality for lung imaging. CT indeed ensures the highest spatial resolution allowing detection of small anomalies such as tiny lung nodules or analyze subtle details such as those encountered in interstitial lung disease. Unfortunately, despite multiple efforts on dose reduction, this modality remains performed at a price of a radiation dose that may be harmful in young patients and/or those requiring multiple follow-up studies. In this setting, the goal of our study was to evaluate if lung imaging could be improved by using HF-NIV with UTE acquisition in comparison with UTE free-breathing imaging and with VIBE breath-hold imaging. The former has the advantage to maintain the patient in apnea-like suppression of respiratory motion while assuring gas exchanges, at full inspiration. Such an exploration at full inspiration may be a major advantage, compared with most free-breathing approaches that acquire data at tidal volumes and to breath-

hold acquisitions, which despite an end-inspiration volume, suffer from a limited resolution.

Indeed, data acquisition at full inspiration has the potential to further increase the detectability of lesions especially at lung bases.[11] Furthermore, in the field of airway imaging, bronchial dimensions may be difficult to ascertain when the airway lumen is collapsed at tidal breathing, or difficult to discriminate from mucus plugging. However, an additional expiration acquisition remains beneficial in this setting in order to assess air trapping, a major finding of small airway disorders. Importantly, with the HF-NIV technique high sharpness was measured close to the diaphragm. This will potentially contribute to improvements of the overall analysis at lung bases, these areas being most susceptible to underrecognition of lesions. In particular, this may be crucial in interstitial diseases, where some patterns such as honeycombing are known to commonly predominate in the periphery of lung bases. Moreover, if lesions may be more easily detected, this technique could also potentially increase the sharpness of their margins, thus allowing a better assessment of their morphologic characteristics as well as their volumetric assessment, when feasible. Comparative patient studies with CT are now required to assess the advantage of MRI using HF-NIV in this context. Evolution of
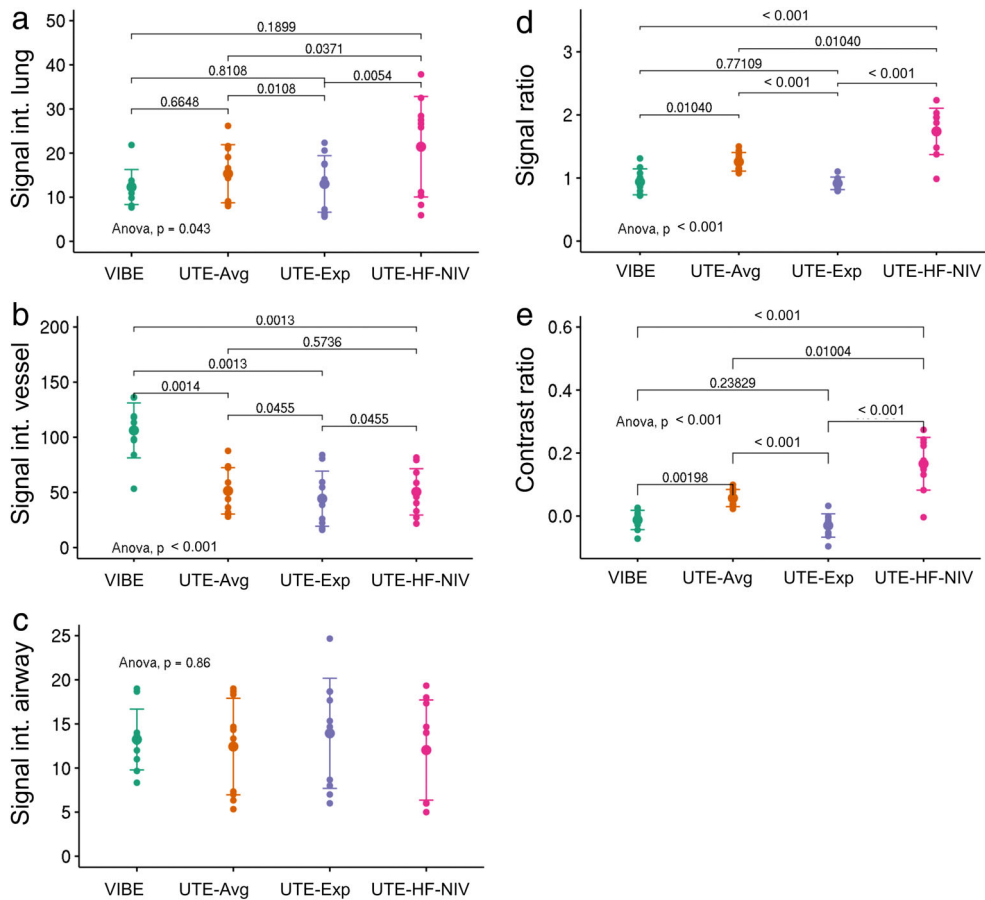
FIGURE 3: Significantly increased average signal intensity with use of HF-NIV in the lung parenchyma (a). Significantly decreased signal intensity compared with VIBE sequences in the vessels (b). No significant differences in airway (c) signal intensities. Resulting significantly higher average apparent signal (d) and contrast (e) ratios with the use of HF-NIV. Error bars indicate standard deviation.

MR techniques may eventually enable high-resolution 3D-UTE of the lung in a couple of seconds in the future. However, to date our results highlight that HF-NIV is an innovative noninvasive technique that enables obtaining the MR appearance of the lung at full inspiration with high spatial resolution, and to investigate it.

Besides the advantage of acquisition at full inspiration, the HF-NIV technique also allowed improvements in image quality, particularly for vessel and airway sharpness of the whole chest. The good-to-excellent interobserver reliability we observed in our study, in combination with the results of previous studies, allow us to use the visual assessment with confidence to evaluate the impact of HF-NIV on image quality. Although the results of software-based vessel sharpness did not highlight a significant average difference with the small sample size, a trend to improvement was observed (Fig. 2d). No improvements were observed in software-based vessel sharpness and lung–liver interface definition for two individuals with the use of HF-NIV compared with the acquisition during FB. This can most likely be attributed to the fact that images acquired in free-breathing for these two subjects exhibited very little motion-related artifacts, as seen, for example, in Fig. 5a,c. In young, healthy, and physically active subjects, breathing is more regular and reproducible and more time is spent in the expiratory part of the respiratory cycle.[31] This factor may cause underestimation of the advantage offered by the HF-NIV procedure. In a patient population with more irregular and less reproducible breathing patterns,[31] the HF-NIV respiratory stabilization procedure most likely should offer increased image quality improvements.

These improvements in sharpness for most subjects with UTE-HF-NIV when compared with VIBE and UTE-FB indicate that HF-NIV could be a viable alternative to current standard acquisitions for chest imaging. In this study, prospective respiratory gating was not used for the free-breathing acquisition, as this would have required prolonged acquisition time to achieve a sampling level identical to the HF-NIV data. A retrospective gating was nevertheless performed; therefore, with an undersampling degree higher than that used for the VIBE, UTE-HF-NIV, and UTE-Avg methods. Therefore, further studies are required to assess the advantage of HF-NIV when compared with gated acquisitions[2,17,23,25,27,32,33] or motion-resolved reconstructions[26] at an equivalent sampling level. While the VIBE acquisition provided a valuable point of reference as a sequence frequently used in clinical practice, further comparisons with optimized breath-hold protocols[34–36] could be of value. Also, additional image quality improvements could be expected in UTE-HF-NIV images if retrospective
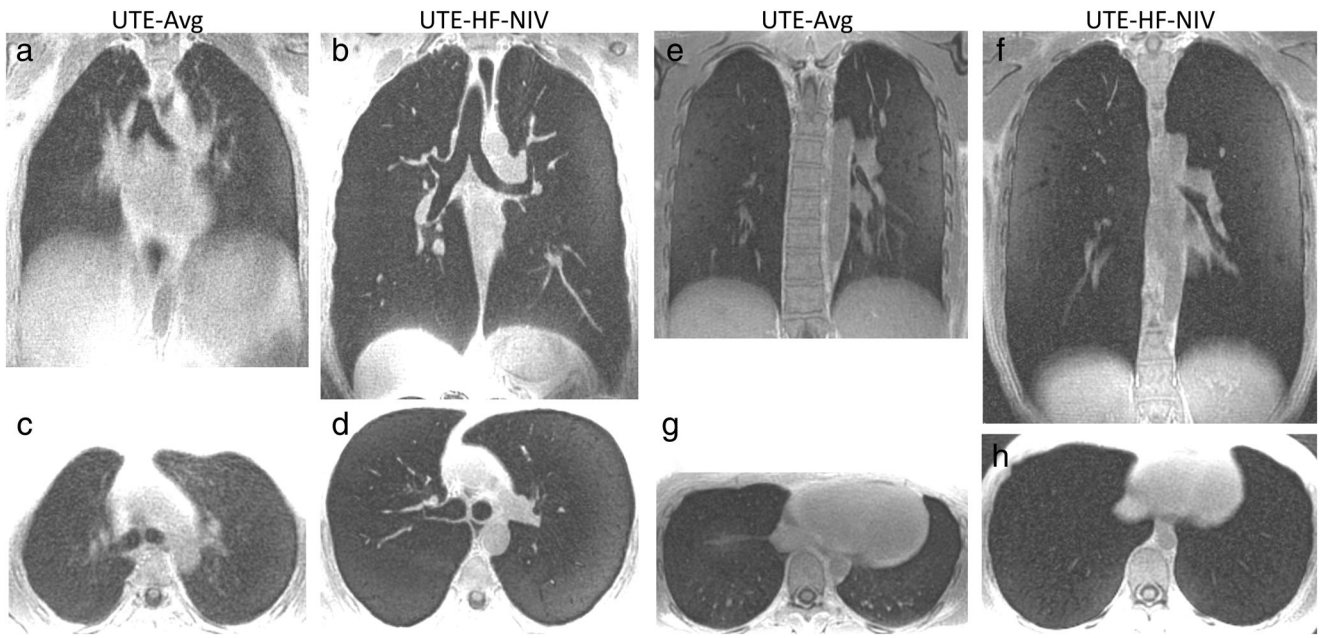
FIGURE 4: Comparison of the two equally sampled UTE acquisitions in a healthy volunteer. (a) Coronal slice of a free-breathing acquisition (UTE-Avg). (b) Coronal slice of an HF-NIV acquisition. (c) Axial slice of a free-breathing acquisition (UTE-Avg). (d) Axial slice of an HF-NIV acquisition. The difference in lung volume can be appreciated visually. Sharper features are observed in images acquired with HF-NIV. Comparison of the two equally sampled UTE acquisitions in another healthy volunteer. (e) Coronal slice of a free-breathing acquisition (UTE-Avg). (f) Coronal slice of an HF-NIV acquisition. (g) Axial slice of a free-breathing acquisition (UTE-Avg). (h) Axial slice of an HF-NIV acquisition. The difference in lung volume can be appreciated visually. For this volunteer, contrary to most other cases, the free-breathing acquisition contained few respiratory motion artifacts. In this case, blurring introduced by the ventilation technique can be observed at the lung bases (f).

gating or motion-resolved reconstructions were used to remove residual motion artifacts linked to the ventilation procedure. Indeed, the variations in diaphragm position should be about 3 mm, quite similar with high-frequency ventilation under anesthesia.[37] Conversely, variations of about 2 cm are expected in FB.
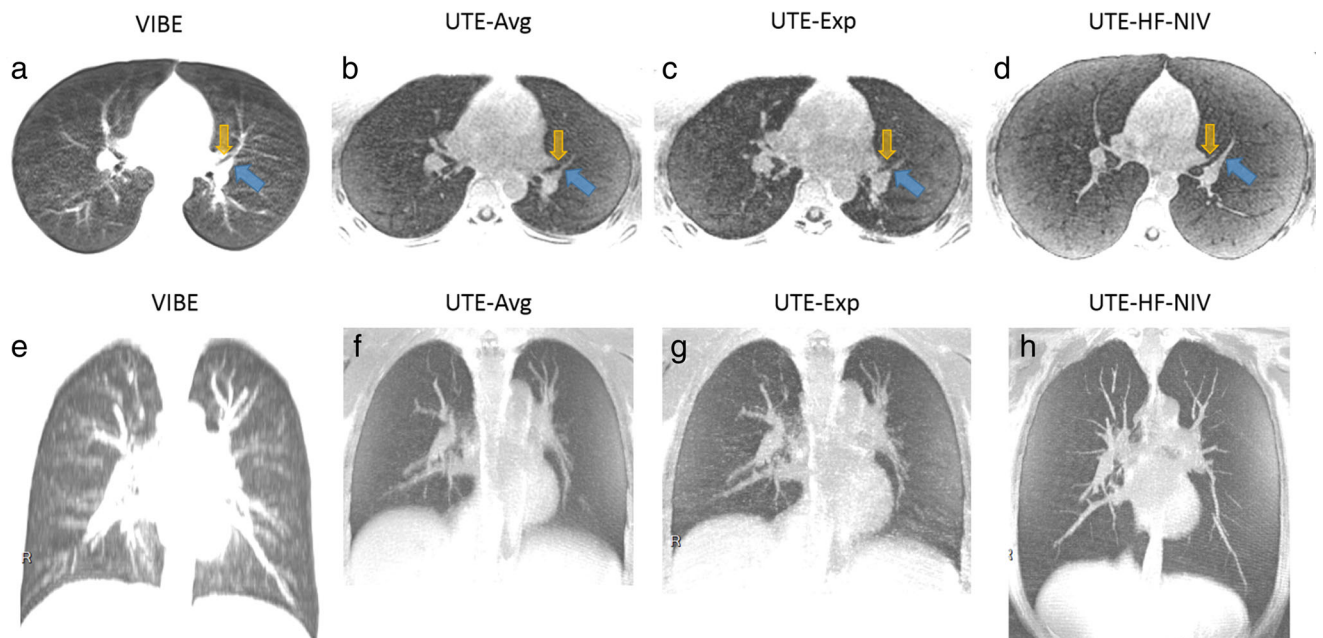
FIGURE 5: Axial 1.30-mm thick slices at the level of the middle lobe and the lingula bronchovascular bundles of a VIBE (a), UTE-Avg (b), UTE-Exp (c), UTE-HF-NIV (d) sequences. The sharpness of vessels such as the pulmonary artery branch of the lingula (blue arrows) is increased, as well as the sharpness of bronchial walls with the UTE-HF-NIV sequence. A 15-mm thick maximum intensity projection reformat in a coronal orientation of a VIBE (e), UTE-Avg (f), UTE-Exp (g), UTE-HF-NIV (h) sequences. Although vessel visibility is similar between various sequences, the sharpness of vessels is increased with the UTE HF-NIV sequence. Note the increased volume of lungs with the same sequence allowing to display the elongated vessels on a large section.

Improvement of airway and vessel sharpness as well as lung–liver interfaces in most volunteers contribute to an improvement in apparent spatial resolution. Therefore, in addition to acquisition at full inspiration, a better individualization of tiny nodules or subtle lesions is expected due to a better delineation of vessel/lung interfaces. In addition, the increase in signal and contrast ratios of the lung parenchyma when using HF-NIV for acquisition compared with free-breathing and breath-hold methods further improve the overall image quality owing to a better visibility of structures as well as contrast towards neighboring structures. This is mostly attributable to the larger signal intensity achieved in the parenchyma as well as the lower signal intensity measured in vessel in images acquired with UTE-HF-NIV compared with VIBE, for instance.

This signal ratio increase could be ascribed to the elevated presence of oxygen during high-frequency ventilation, as oxygen can act as a T_1 shortening agent.[38] Also, the HF-NIV technique allows a decrease in motion-related artifacts: the use of the HF-NIV method may have suppressed data inconsistencies related to imperfect motion correction, even by using advanced retrospective reconstruction. These data inconsistencies are a major drawback of all conventional respiratory synchronization systems such as respiratory belt or navigator. These inconsistencies create data undersampling and therefore undersampling artifacts, which are not always fully compensated or corrected. By using the HF-NIV method, a substantial reduction of the undersampling degree may have been allowed compared with standard motion-correction techniques and, thus, enables higher signal ratio and contrast ratio values.

There are some limitations in our study. In particular, these results were obtained on a small sample of healthy volunteers. While the application of HF-NIV in a patient setting has already been studied for radiotherapy[15] and positron emission tomography (PET) imaging,[39] patient studies are still required for MRI. In this population, more irregular and less reproducible breathing patterns are expected. Finally, the acquisition with HF-NIV was performed at full inspiration, conversely to FB, which is carried out at tidal volumes, and this could change the overall visual evaluation of image quality. However, software-based evaluations were not influenced by the lung volume. Furthermore, the potential benefit of the technique for MR techniques other than UTE, such as diffusion or contrast MR sequences, remains to be investigated. These complementary sequences may also potentially benefit from the lack of motion correction during the acquisition to reach faster and/or better performance.

Furthermore, since this study focused on evaluating the benefits of image quality for MRI in healthy volunteers, another limitation is that no comparisons with other imaging modalities such as CT were made. In this study population, for ethical reasons, the use of ionizing radiation was not possible. Further studies in patients are therefore required to ascertain the performance of MRI using HF-NIV in comparison with modalities currently used clinically.

In conclusion, the HF-NIV technique allows an overall significant improvement in image quality for lung imaging with UTE sequences compared with FB. The approach further affords the advantage of exploring the lung under an apnea-like condition at full inspiration, ie, in a ventilation state similar to that commonly used in CT lung exams. Although these findings require confirmation in a larger cohort, this may offer a realistic option to alternate between MRI and CT during follow-up studies, which may ultimately help reduce the cumulative radiation dose.

Acknowledgment

References

1. Bergin CJ, Pauly JM, Macovski A. Lung parenchyma: Projection reconstruction MR imaging. Radiology 1991;179:777–781.

2. Johnson KM, Fain SB, Schiebler ML, Nagle S. Optimized 3D ultrashort echo time pulmonary MRI. Magn Reson Med 2013;70:1241–1250.

3. Ohno Y, Koyama H, Yoshikawa T, et al. Standard-, reduced-, and no-dose thin-section radiologic examinations: Comparison of capability for nodule detection and nodule type assessment in patients suspected of having pulmonary nodules. Radiology 2017;284:562–573.

4. Burris NS, Johnson KM, Larson PE, et al. Detection of small pulmonary nodules with ultrashort echo time sequences in oncology patients by using a PET/MR system. Radiology 2016;278:239–246.

5. Wielputz MO, Lee HY, Koyama H, et al. Morphologic characterization of pulmonary nodules with ultrashort TE MRI at 3T. AJR Am J Roentgenol 2018;210:1216–1225.

6. Dournes G, Menut F, Macey J, et al. Lung morphology assessment of cystic fibrosis using MRI with ultra-short echo time at submillimeter spatial resolution. Eur Radiol 2016;26:3811–3820.

7. Chang EY, Du J, Chung CB. UTE imaging in the musculoskeletal system. J Magn Reson Imaging 2015;41:870–883.

8. Wild JM, Marshall H, Bock M, et al. MRI of the lung (1/3): Methods. Insights Imaging 2012;3:345–353.

9. Lederlin M, Cremillieux Y. Three-dimensional assessment of lung tissue density using a clinical ultrashort echo time at 3 Tesla: A feasibility study in healthy subjects. J Magn Reson Imaging 2014;40:839–847.

10. Triphan SM, Breuer FA, Gensler D, Kauczor HU, Jakob PM. Oxygen enhanced lung MRI by simultaneous measurement of T1 and T2* during free breathing using ultrashort TE. J Magn Reson Imaging 2015;41:1708–1714.

11. Allen-Auerbach M, Yeom K, Park J, Phelps M, Czernin J. Standard PET/CT of the chest during shallow breathing is inadequate for comprehensive staging of lung cancer. J Nucl Med 2006;47:298–301.

12. Biederer J, Beer M, Hirsch W, et al. MRI of the lung (2/3). Why… when… how? Insights Imaging 2012;3:355–371.

13. Taylor AM, Jhooti P, Wiesmann F, Keegan J, Firmin DN, Pennell DJ. MR navigator-echo monitoring of temporal changes in diaphragm position: Implications for MR coronary angiography. J Magn Reson Imaging 1997;7:629–636.

14. Wang Y, Rossman PJ, Grimm RC, Wilman AH, Riederer SJ, Ehman RL. 3D MR angiography of pulmonary arteries using realtime navigator gating and magnetization preparation. Magn Reson Med 1996;36: 579–587.

15. Peguret N, Ozsahin M, Zeverino M, et al. Apnea-like suppression of respiratory motion: First evaluation in radiotherapy. Radiother Oncol 2016;118:220–226.

16. Beigelman-Aubry C, Peguret N, Stuber M, et al. Chest-MRI under pulsatile flow ventilation: A new promising technique. PLoS One 2017;12: e0178807.

17. Delacoste J, Chaptinel J, Beigelman-Aubry C, Piccini D, Sauty A, Stuber M. A double echo ultra short echo time (UTE) acquisition for respiratory motion-suppressed high resolution imaging of the lung. Magn Reson Med 2018;79:2297–2305.

18. Nielles-Vallespin S, Weber MA, Bock M, et al. 3D radial projection technique with ultrashort echo times for sodium MRI: Clinical applications in human brain and skeletal muscle. Magn Reson Med 2007;57: 74–81.

19. Piccini D, Littmann A, Nielles-Vallespin S, Zenge MO. Spiral phyllotaxis: The natural way to construct a 3D radial trajectory in MRI. Magn Reson Med 2011;66:1049–1056.

20. Ogna A, Bernasconi M, Belmondo B, et al. Prolonged apnea supported by high-frequency noninvasive ventilation: A pilot study. Am J Respir Crit Care Med 2017;195:958–960.

21. Ogna A, Ambrosi X, Prigent H, et al. Use of home ventilators for ventilatory support during magnetic resonance imaging. Austin J Pulm Respir Med 2016;3:1040.

22. Feng L, Delacoste J, Smith D, et al. Simultaneous evaluation of lung anatomy and ventilation using 4D respiratory-motion-resolved ultrashort echo time sparse MRI. J Magn Reson Imaging 2019;49:411–422.

23. Ohno Y, Koyama H, Yoshikawa T, et al. Pulmonary high-resolution ultrashort TE MR imaging: Comparison with thin-section standard- and low-dose computed tomography for the assessment of pulmonary parenchyma diseases. J Magn Reson Imaging 2016;43:512–532.

24. Etienne A, Botnar RM, Van Muiswinkel AM, Boesiger P, Manning WJ, Stuber M. "Soap-Bubble" visualization and quantitative analysis of 3D coronary magnetic resonance angiograms. Magn Reson Med 2002;48: 658–666.

25. Tibiletti M, Paul J, Bianchi A, et al. Multistage three-dimensional UTE lung imaging by image-based self-gating. Magn Reson Med 2016;75: 1324–1332.

26. Jiang W, Ong F, Johnson KM, et al. Motion robust high resolution 3D free-breathing pulmonary MRI using dynamic 3D image self-navigator. Magn Reson Med 2018;79:2954–2967.

27. Dournes G, Grodzki D, Macey J, et al. Quiet submillimeter MR imaging of the lung is feasible with a PETRA sequence at 1.5T. Radiology 2015; 276:258–265.

28. Holm S. A simple sequentially rejective multiple test procedure. Scand J Statist, Wiley, 1979;6:65–70.

29. Wongpakaran N, Wongpakaran T, Wedding D, Gwet KL. A comparison of Cohen's Kappa and Gwet's AC1 when calculating inter-rater reliability coefficients: A study conducted with personality disorder samples. BMC Med Res Methodol 2013;13:61.

30. Shankar V, Bangdiwala SI. Observer agreement paradoxes in 2x2 tables: Comparison of agreement measures. BMC Med Res Methodol 2014;14:100.

31. Ginami G, Bonanno G, Schwitter J, Stuber M, Piccini D. An iterative approach to respiratory self-navigated whole-heart coronary MRA significantly improves image quality in a preliminary patient study. Magn Reson Med 2016;75:1594–1604.

32. Dournes G, Yazbek J, Benhassen W, et al. 3D ultrashort echo time MRI of the lung using stack-of-spirals and spherical k-space coverages: Evaluation in healthy volunteers and parenchymal diseases. J Magn Reson Imaging 2018 [Epub ahead of print].

33. Higano NS, Hahn AD, Tkach JA, et al. Retrospective respiratory self-gating and removal of bulk motion in pulmonary UTE MRI of neonates and adults. Magn Reson Med 2017;77:1284–1295.

34. Bieri O. Ultra-fast steady state free precession and its application to in vivo (1)H morphological and functional lung imaging at 1.5 Tesla. Magn Reson Med 2013;70:657–663.

35. Heye T, Sommer G, Miedinger D, Bremerich J, Bieri O. Ultrafast 3D balanced steady-state free precession MRI of the lung: Assessment of anatomic details in comparison to low-dose CT. J Magn Reson Imaging 2015;42:602–609.

36. Sheikh K, Guo F, Capaldi DP, et al., Canadian Respiratory Research N. Ultrashort echo time MRI biomarkers of asthma. J Magn Reson Imaging 2017;45:1204–1215.

37. Denys A, Lachenal Y, Duran R, Chollet-Rivier M, Bize P. Use of high-frequency jet ventilation for percutaneous tumor ablation. Cardiovasc Intervent Radiol 2014;37:140–146.

38. Edelman RR, Hatabu H, Tadamura E, Li W, Prasad PV. Noninvasive assessment of regional ventilation in the human lung using oxygen-enhanced magnetic resonance imaging. Nat Med 1996;2:1236–1239.

39. Prior JO, Peguret N, Pomoni A, et al. Reduction of respiratory motion during PET/CT by pulsatile-flow ventilation: A first clinical evaluation. J Nucl Med 2016;57:416–419.